

CALIS - a CALibration Insertion System for the DarkSide-50 dark matter search experiment

P. Agnes^a, T. Alexander^{ae}, A. Alton^b, K. Arisaka^{ad}, H.O. Back^x,
B. Balding^g, K. Biery^g, G. Bonfini^q, M. Bossaⁱ, A. Brigatti^s, J. Brodsky^x,
F. Budano^y, L. Cadonati^{ae}, F. Calaprice^x, N. Canci^{ad}, A. Candela^q,
H. Cao^x, M. Cariello^h, P. Cavalcante^q, A. Chavarria^d, A. Chepurnov^t,
A.G. Cocco^u, L. Crippa^s, D. D'Angelo^s, M. D'Incecco^q, S. Davini^k,
M. De Deo^q, A. Derbin^v, A. Devoto^c, F. Di Eusonio^x, G. Di Pietro^s,
E. Edkins^j, A. Empl^k, A. Fan^{ad}, G. Fiorillo^u, K. Fomenko^f, G. Forster^{ae},
D. Franco^a, F. Gabriele^q, C. Galbiati^x, A. Goretti^x, L. Grandi^d,
M. Gromov^t, M.Y. Guan^l, Y. Guardincerri^g, B. Hackett^j, K. Herner^g,
E.V. Hungerford^k, Al. Ianni^q, An. Ianni^x, C. Jollet^{aa}, K. Keeter^e,
C. Kendziora^g, S. Kidner^{af,1}, V. Kobylevⁿ, G. Koh^x, D. Korablev^f,
G. Korga^k, A. Kurlej^{ae}, P.X. Li^l, B. Loer^x, P. Lombardi^s, C. Love^{ab},
L. Ludhova^s, S. Luitz^z, Y.Q. Ma^l, I. Machulin^{o,r}, A. Mandaranoⁱ, S. Mari^y,
J. Maricic^j, L. Marini^y, C.J. Martoff^{ab}, A. Meregaglia^{aa}, E. Meroni^s,
P.D. Meyers^{x,*}, R. Milincic^j, D. Montanari^g, A. Monte^{ae}, M. Montuschi^q,
M.E. Monzani^z, P. Mosteiro^x, B. Mount^e, V. Muratova^v, P. Musico^h,
A. Nelson^x, S. Odrowski^q, M. Okounkova^x, M. Orsini^q, F. Ortica^w,
L. Pagani^h, M. Pallavicini^h, E. Pantic^{ad,ac}, L. Papp^{af}, S. Parmeggiano^s,
R. Parsells^x, K. Pelczar^m, N. Pelliccia^w, S. Perasso^a, A. Pocar^{ae},
S. Pordes^g, D. Pugachev^o, H. Qian^x, K. Randle^{ae}, G. Ranucci^s,
A. Razeto^q, B. Reinhold^j, A. Renshaw^{ad}, A. Romani^w, B. Rossi^{x,u},
N. Rossi^q, S.D. Rountree^{af}, D. Sablone^k, P. Saggese^q, R. Saldanha^d,
W. Sands^x, S. Sangiorgio^p, E. Segreto^q, D. Semenov^v, E. Shields^x,
M. Skorokhvatov^{o,r}, O. Smirnov^f, A. Sotnikov^f, C. Stanford^x,
Y. Suvorov^{ad}, R. Tartaglia^q, J. Tatarowicz^{ab}, G. Testera^h, A. Tonazzo^a,
E. Unzhakov^v, R.B. Vogelaar^{af}, M. Wada^x, S. Walker^u, H. Wang^{ad},
Y. Wang^l, A. Watson^{ab}, S. Westerdale^x, M. Wojcik^m, A. Wright^x,
X. Xiang^x, J. Xu^x, C.G. Yang^l, J. Yoo^g, S. Zavatarelli^h, A. Zec^{ae}, C. Zhu^x,
G. Zuzel^{lm}

*Corresponding authors.

Email address: meyers@princeton.edu (P.D. Meyers)

¹Deceased

- ^a*APC, Université Paris Diderot, Sorbonne Paris Cité, Paris 75205, France*
- ^b*Physics and Astronomy Department, Augustana College, Sioux Falls, SD 57197, USA*
- ^c*Physics Department, Università degli Studi and INFN, Cagliari 09042, Italy*
- ^d*Kavli Institute, Enrico Fermi Institute and Dept. of Physics, University of Chicago, Chicago, IL 60637, USA*
- ^e*School of Natural Sciences, Black Hills State University, Spearfish, SD 57799, USA*
- ^f*Joint Institute for Nuclear Research, Dubna 141980, Russia*
- ^g*Fermi National Accelerator Laboratory, Batavia, IL 60510, USA*
- ^h*Physics Department, Università degli Studi and INFN, Genova 16146, Italy*
- ⁱ*Gran Sasso Science Institute, L’Aquila 67100, Italy*
- ^j*Department of Physics and Astronomy, University of Hawai’i, Honolulu, HI 96822, USA*
- ^k*Department of Physics, University of Houston, Houston, TX 77204, USA*
- ^l*Institute of High Energy Physics, Beijing 100049, China*
- ^m*Smoluchowski Institute of Physics, Jagiellonian University, Krakow 30059, Poland*
- ⁿ*Institute for Nuclear Research, National Academy of Sciences of Ukraine, Kiev 03680, Ukraine*
- ^o*National Research Centre Kurchatov Institute, Moscow 123182, Russia*
- ^p*Lawrence Livermore National Laboratory, 7000 East Avenue, Livermore, CA 94550*
- ^q*Laboratori Nazionali del Gran Sasso, Assergi (AQ) 67010, Italy*
- ^r*National Research Nuclear University MEPhI (Moscow Engineering Physics Institute), 115409 Moscow, Russia*
- ^s*Physics Department, Università degli Studi and INFN, Milano 20133, Italy*
- ^t*Skobeltsyn Institute of Nuclear Physics, Lomonosov Moscow State University, Moscow 119991, Russia*
- ^u*Physics Department, Università degli Studi Federico II and INFN, Napoli 80126, Italy*
- ^v*St. Petersburg Nuclear Physics Institute, Gatchina 188350, Russia*
- ^w*Chemistry, Biology and Biotechnology Department, Università degli Studi and INFN, Perugia 06123, Italy*
- ^x*Department of Physics, Princeton University, Princeton, NJ 08544, USA*
- ^y*Physics Department, Università degli Studi Roma Tre and INFN, Roma 00146, Italy*
- ^z*SLAC National Accelerator Laboratory, Menlo Park, CA 94025, USA*
- ^{aa}*IPHC, Université de Strasbourg, CNRS/IN2P3, Strasbourg 67037, France*
- ^{ab}*Physics Department, Temple University, Philadelphia, PA 19122, USA*
- ^{ac}*Physics Department, University of California, Davis, CA 95616, USA*
- ^{ad}*Physics and Astronomy Department, University of California, Los Angeles, CA 90095, USA*
- ^{ae}*Amherst Center for Fundamental Interactions and Physics Department, University of Massachusetts, Amherst, MA 01003, USA*
- ^{af}*Physics Department, Virginia Tech, Blacksburg, VA 24061, USA*

Abstract

In order to calibrate the detector response and detection efficiency of the DarkSide-50 Liquid Argon Time Projection Chamber used for dark

matter detection and the surrounding 30 t organic liquid scintillator neutron veto, we designed, built and implemented a calibration source insertion system (CALIS), which allows to deploy radioactive sources into the liquid scintillator veto. It was commissioned in September 2014 and used successfully in several campaigns to deploy gamma and neutron sources since then. A description of the hardware and highlights from calibration analysis results are given below.

Keywords:

Dark matter, WIMP, Noble liquid detectors, Low-background detectors, Liquid scintillators, radioactive source calibration

PACS: 95.35.+d, 29.40.Mc, 29.40Gx

1 Contents

2 1 Introduction	4
3 2 Design Requirements & Hardware Implementation	4
2.1 Purpose	4
2.2 Deployment & Articulation Mechanism	6
2.3 Housing & Scintillator	9
2.4 Deployment device	11
2.5 Source holder and arms	12
2.6 Hardware details and safety features	12
2.7 Degrees of freedom of the system	14
11 3 Testing, Cleaning and Commissioning	16
12 4 Calibration Campaigns	17
4.1 Radioactive Sources	17
4.2 Timeline of the Calibration Campaigns and Stability	18
4.3 TPC Calibration	19
4.4 Liquid Scintillator Veto	22
17 5 Conclusions	23

18 **1. Introduction**

19 DarkSide-50 is a Liquid Argon Time Projection Chamber (LAr TPC),
20 operated in the Gran Sasso National Laboratory (LNGS) in Italy to search
21 for nuclear recoils induced by weakly interacting massive particles (WIMPs).
22 A first physics result was reported in [1] based on 50 live days of data col-
23 lected with Atmospheric Argon (AAr), providing the most sensitive limit
24 on a dark matter search using a LAr TPC to date with a 90% CL upper
25 limit on the WIMP-nucleon spin-independent cross section of 6.1×10^{-44}
26 cm^2 for a WIMP mass of 100 GeV/c².

27 The DarkSide-50 apparatus has been described in detail in [1], but for
28 the reader's convenience a short reminder is given. As shown in fig. 1
29 it features a LAr TPC surrounded by a 30 t liquid scintillator-based veto
30 (LSV) system, which in turn is housed in a water Cerenkov veto (WCV),
31 both of which help to measure in-situ and suppress radiogenic and cos-
32 mogenic backgrounds. On top of the WCV there is a radon-free clean
33 room (CRH) which houses the cryogenic supply system, the electronics
34 and slow control software, among other things (Fig. 2). The inside of the
35 LSV is accessible from CRH through four access ports nick named organ
36 pipes, which end at their top in gate valves.

37 *Laser calibration*

38 Electronics gain calibration of the WCV, LSV and TPC is done with
39 dedicated Laser systems, that are in place in each of the three subdetec-
40 tors. The Laser calibration in the WCV is sufficient to veto muons (and
41 their secondaries) with high efficiency [2]. The TPC detector response
42 has been calibrated using the internal ³⁹Ar as well as ^{83m}Kr, that has
43 been added into the LAr recirculation system during dedicated calibra-
44 tion campaigns [1].

45 **2. Design Requirements & Hardware Implementation**

46 **2.1. Purpose**

47 The goal with the CALibration source Insertion System (CALIS) is to
48 study and calibrate the detector response of the TPC and the LSV as well
49 as the detection efficiency of internal neutrons interacting in the TPC and
50 LSV using radioactive gamma and neutron sources. This complements

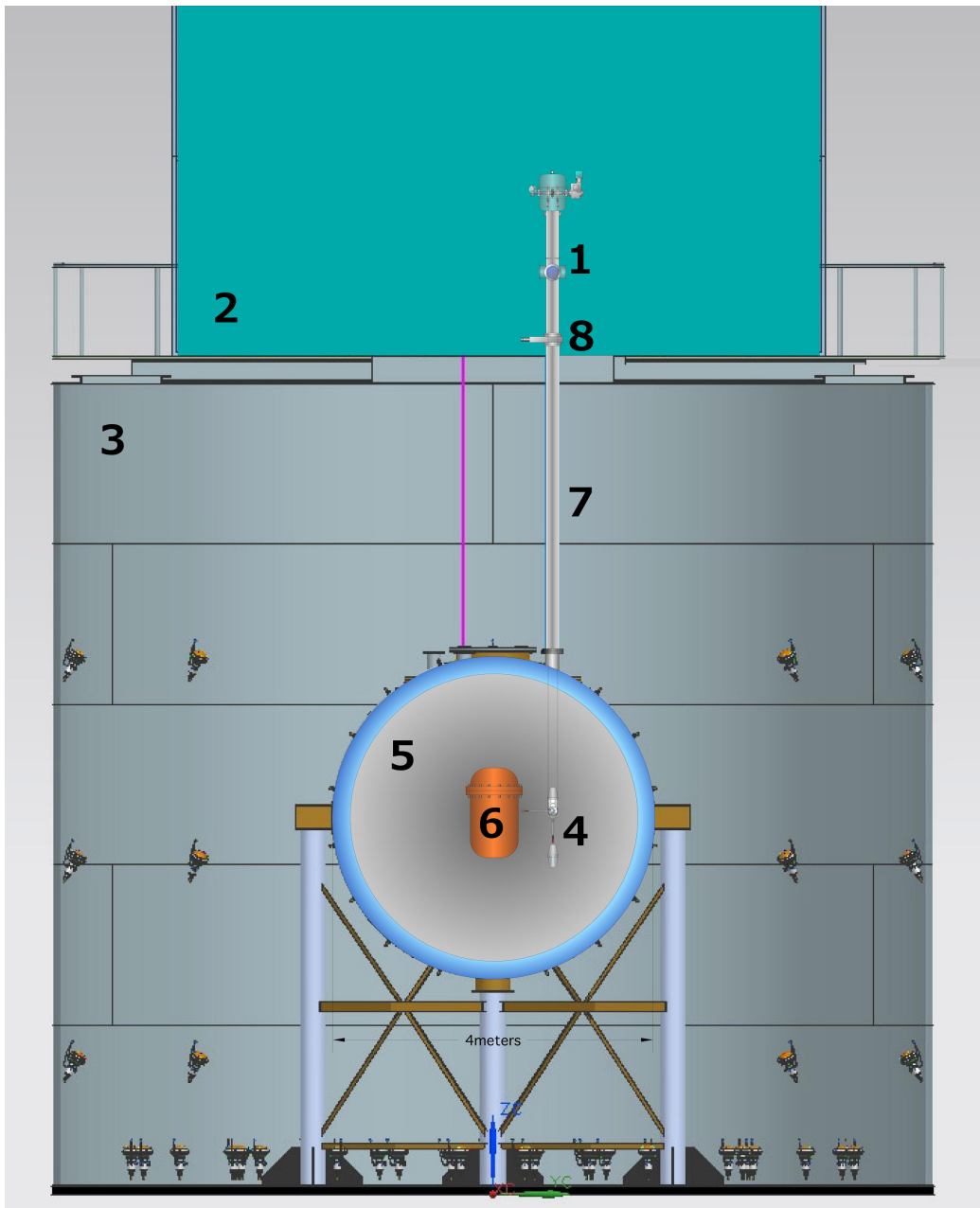


Figure 1: A conceptual drawing of CALIS (1) installed in the radon-free clean room CRH (2) atop the water Cerenkov veto (WCV, 3) and with the deployment device (4) containing the source deployed in the liquid scintillator veto (LSV, 5) next to the liquid argon time projection chamber's (LAr TPC) cryostat (6). The clean room and the LSV are connected through four access ports nick named organ pipes (only one of which is drawn in the sketch above: (7)). All four organ pipes end in CRH at gate valves (8) which can be manually opened or closed. During normal operations all four organ pipes are closed. Not included in the sketch are tubes connecting the cryogenic systems in CRH to the cryostat in the LSV [2].

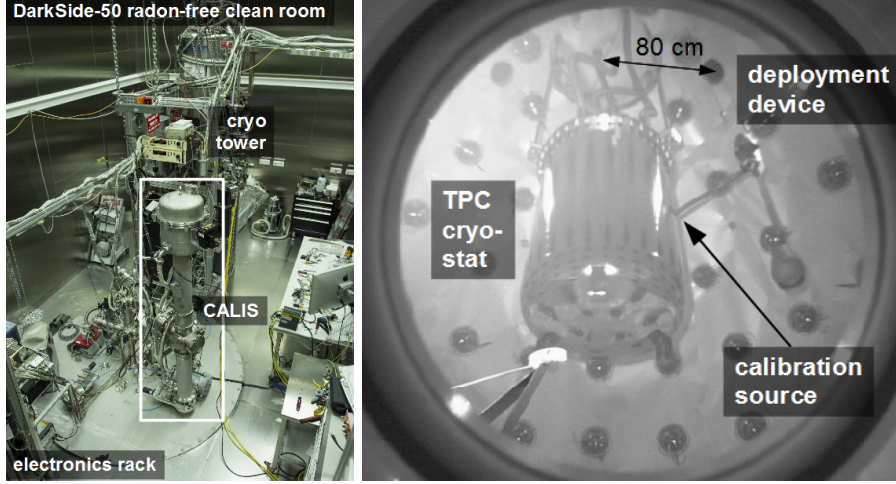


Figure 2: *left*: CALIS after installation inside the radon-free clean room CRH. The organ pipe is 80 cm off-center with respect to the TPC center in the horizontal XY plane. *right*: Photograph taken with a camera looking upwards into the LSV from the bottom. It shows the source deployment device deployed through one of the organ pipes visible on the top right. The arm is articulated and the source is next to the cryostat of the LAr TPC [2].

51 and extends the physics reach of internal calibration sources and Laser
52 calibration.

53 The center of the LSV is about 6 m below the gate valve inside CRH
54 and the 6" wide organ pipes are vertical, yet about 80 cm off center in the
55 XY plane as shown in Fig. 2. For TPC calibration the radioactive source
56 has to be positioned in immediate contact with the cryostat, in order
57 to minimize rate losses through absorption in particular for low energy
58 sources such as ^{57}Co (122 keV).

59 2.2. Deployment & Articulation Mechanism

60 This requirement precludes a single cable solution deployed from
61 within a glove box as has been used in several scintillator experiments
62 [3, 4] Instead the apparatus consists of the housing, which has been in-
63 stalled in CRH (Fig. 2, left) and the deployment device is attached to the
64 housing through two stainless steel cables that are wound up on cable
65 spools and allow the lowering of the device into the LSV, next to the
66 cryostat (Fig. 2, right).

67 The stepper motor moves both cable spools concurrently and sends
68 the deployment device into the LSV. An absolute encoder provides its

in fig.3 the drawing should show the the arm articulate towards the left, since when the left spool is engaged, the arm articulates towards the left.

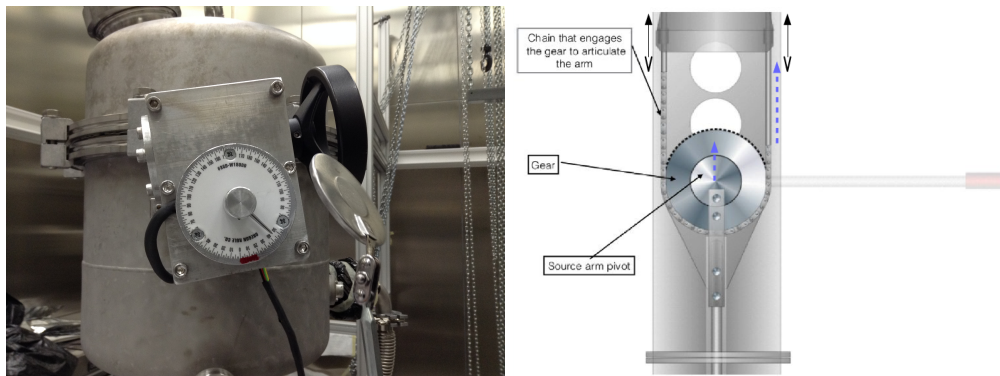
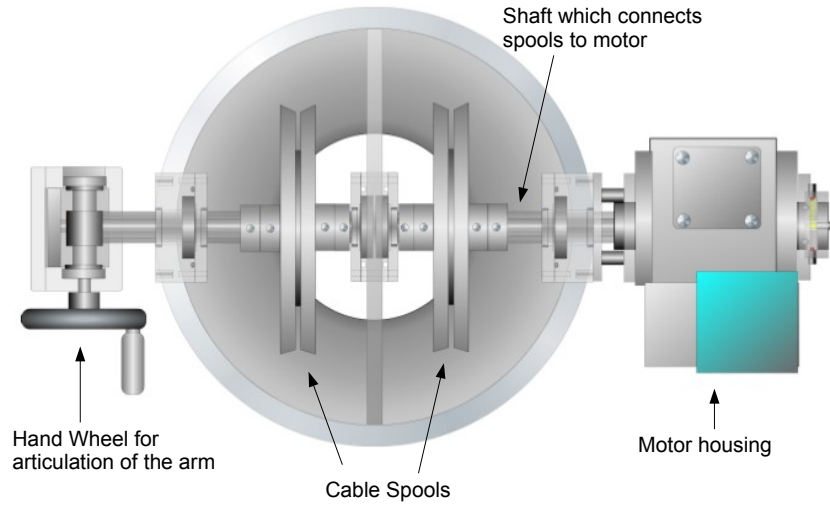


Figure 3: *top*: Inside view of the drive mechanism's components seen from the top of CALIS. The stepper motor inside the motor housing drives both cable spools concurrently, thereby lowering the calibration device into the LSV. An absolute encoder provides the current position of the deployment device. The hand wheel on the left turns the left spool only (*bottom left*). When engaged, it drives the gear to transfer the rotation of the articulation wheel into a rotation of the source arm (*bottom right*). The chain has a guard rail, not shown in the drawing, that ensures that the chain can never come off the gear.

69 current position, even in the absence of power. The stepper motor is
 70 controlled via a simple graphical LabVIEW interface, run on a dedicated
 71 laptop, in which the current z-position is shown and a target z-position
 72 can be provided by the operator. Z-positions are given in motor step
 73 counts, an arbitrary unit which has been calibrated outside CRH in meters
 74 (Fig. 4) and relative to the TPC using the t-drift distribution of calibration
 75 data (Fig. 13, p. 22).

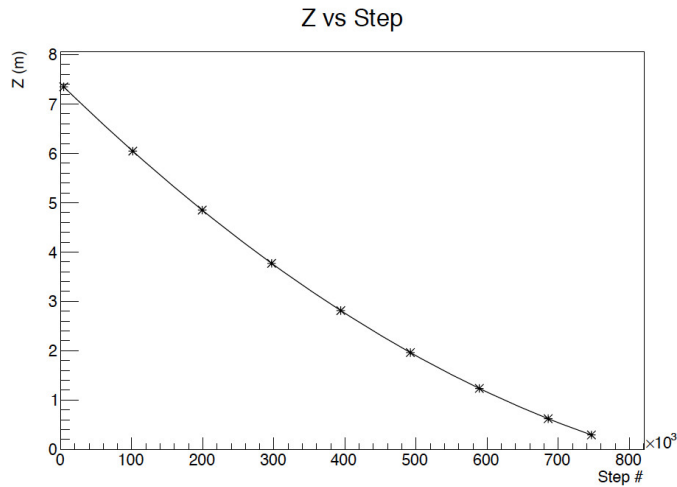


Figure 4: Plot of the z position of the deployment device versus the step position of the motor. The non-linear correspondence between the number of steps and the length of cable deployed arises as follows: As the cable winds around the spool, the winding radius changes, increasing as the pig is lifted and decreasing as it is lowered. A motor step count corresponds to a fixed angular distance $d\theta$, yet the amount of cable deployed during this motor step count is *winding radius* $\cdot d\theta$. As the winding radius changes as a function of z position, the fraction of deployed cable per motor step count changes.

76 Articulation of the arm is done manually via the articulation wheel.
 77 This affects only the cable spool close to the articulation wheel, the left
 78 one in Fig. 3, thereby shortening the left cable with respect to the right
 79 cable and engaging the gear through a chain (Fig. 3). As a result the arm
 80 is articulated and the pivot center is lifted. The non-linearity arising from
 81 the change in winding radius on the cable spools affects also the amount
 82 of rotation required by the hand wheel for horizontal articulation of the
 83 source arm. The degrees corresponding to a horizontal articulation has
 84 been calibrated as a function of cable length deployed prior to installation
 85 in CRH.

86 Articulation and a movement in z-direction are mutually exclusive
87 since the articulation of the arm leads to more wound up cable on the
88 spool close to the articulation wheel with respect to the other. If then in
89 deployment mode both spools would be rotated simultaneously with the
90 same angular speed, the cable close to the articulation wheel would wind
91 up faster than the other, which would lead to a build up of difference
92 in cable length and the deployment device would only be hanging on
93 one cable. In order to avoid an imbalanced z-movement the arm has
94 to be dearticulated fully before a change in z-position can be initiated.
95 This is enforced by an electric switch preventing z-movement, which is
96 disengaged only when the arm is fully dearticulated (vertical).

97 *2.3. Housing & Scintillator*

98 Besides providing mechanical support for the deployment device via
99 the cable spools, the housing is the important interface between the radon-
100 free clean room CRH and the LSV, through which sources are exchanged,
101 while protecting the liquid scintillator and avoiding human contact with
102 even traces of liquid scintillator vapor at all times (Fig. 5). It plays the
103 same role as a glove box for other calibration systems yet with a narrower
104 foot print inside CRH. The liquid scintillator is a mixture of PC and TMB²
105 with the wavelength shifter PPO [2]. It may not get exposed to oxygen or
106 water as is present in normal clean room air and also contamination with
107 ²²²Rn and its long-lived radioactive daughters has to be avoided.

108 Starting at the gate valve inside the clean room CRH on which CALIS
109 has been installed, a teflon disk allows to electrically isolate CALIS from
110 ground, even though during normal operations the CALIS housing is also
111 connected to ground. A tripod with a bellow has been used to vertically
112 align the housing right after installation on the gate valve. The bellow is
113 connected to a 23.375" long cylindrical stainless steel enclosure pipe. It
114 has the same diameter as the organ pipe (6") and is connected with the
115 view port by a ring clamp, which plays a critical role in XY rotations (see
116 Sec. 2.7.1). The view port can be opened for handling the source arm and
117 exchanging sources. Everything above the ring clamp forms the upper
118 assembly. It features a stainless steel cylindrical enclosure that houses the
119 cable drive mechanism, including the cable spools the stepper motor and

²The concentration of TMB has varied during campaigns (see Sec. 4).

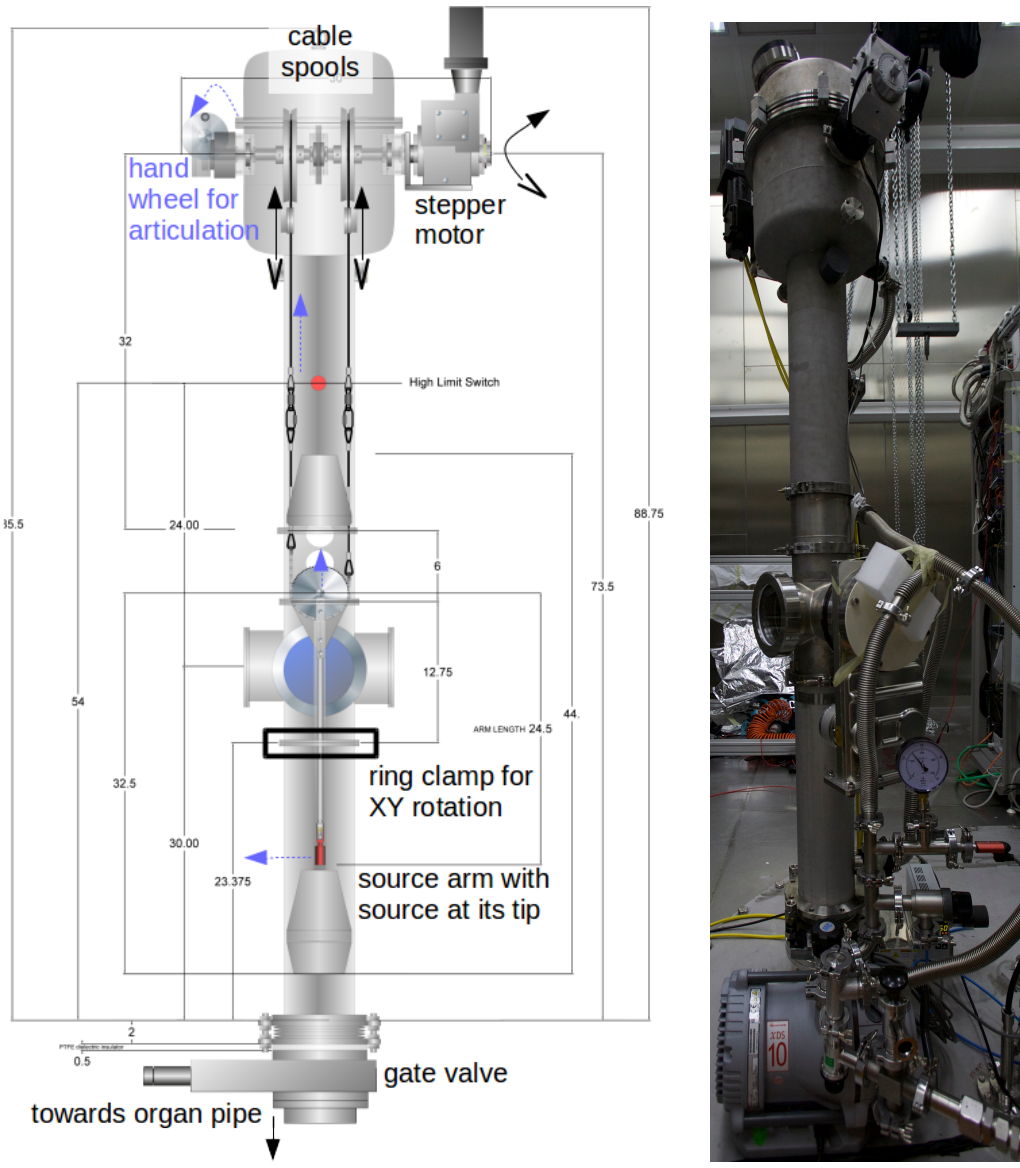


Figure 5: Mechanical drawing of CALIS showing the housing and the deployment device in its home position. Dimensions are in inches. (The total height of 88.75 inches corresponds to 225.4 cm.) The two modes of operation are illustrated: In order to move the deployment device down into the LSV or back up the stepper motor moves both cable spools simultaneously. In order to articulate, the articulation wheel is rotated manually, which affects only the left spool, thereby shortening the left cable with respect to the right cable thereby articulating the arm and lifting the pivot center. The amount of lifting and the amount of rotations until a horizontal articulation is reached has been calibrated prior to installation in CRH (Sec. 3)

120 the articulation mechanism already described in Sec. 2.2.

121 *Vacuum evacuation (flushing) and nitrogen purging*

122 One of the most important safety features of this system is making
123 sure that the TMB and PC residue on the device are extracted from CALIS
124 prior to opening access ports to exchange source or arms. This is impor-
125 tant for safe working level of the operators as well as for the scintillator
126 and radiopurity.

127 After the insertion of the source arm and closure of the view port the
128 inside of the CALIS housing is filled with normal air, that is dangerous to
129 the scintillator. A sequence of evacuations and nitrogen purges reduces
130 the fraction of air including its contaminants (water vapor, oxygen, ra-
131 dioactivity) to negligible levels. Only after this sequence the gate valve is
132 opened and the deployment device is introduced into the LSV. Evacua-
133 tion is achieved with a vacuum pump and exhaust air is removed through
134 dedicated vent lines (Fig. 5).

135 At the end of a calibration campaign, after the deployment device has
136 returned in its home position inside the housing and the gate valve has
137 been closed, scintillator vapor and in particular TMB has to be removed
138 prior to opening the view port. Again a sequence of evacuations and
139 nitrogen purges is employed. By lowering the pressure inside of CALIS
140 below the vapor pressure of TMB and PC, the scintillator gasses out and
141 gets removed through the vent line of the vacuum pump. Once the pres-
142 sure inside the housing stays consistently below the vapor pressure of
143 TMB all scintillator has been removed and the view port can be opened
144 to access the source arm.

145 *Material compatibility*

146 All materials that come in contact with the scintillator veto are made
147 of stainless steel and teflon except for the sealing o-rings which are made
148 of viton. All three materials are certified materials for contact with scin-
149 tillator components TMB and PC.

150 *2.4. Deployment device*

151 The deployment device (Fig. 5) contains the support structure for the
152 arm which holds the source at its end. This piece is equipped with ta-
153 pered cones on the top and bottom that ensure that the ends do not get
154 snagged on inner edges of the organ pipe as it is moving up and down.

155 It is attached to the housing by two cables. Swivel hooks are employed
156 in the attachment of the cables to the pig that allow the cables to move
157 freely and not get tangled. There are two weights built into the device,
158 one cylindrical in the conical cap above the rotation gear mechanism and
159 one inside the cones at the bottom end of the device. Both help to min-
160 imize any lateral motion or oscillations during deployment and articula-
161 tion and dearticulation especially. It also ensures smooth motion of the
162 deployment device into the organ pipe and back to the home position
163 inside the housing.

164 *2.5. Source holder and arms*

165 A source arm and the source holder are attached to the articulation
166 gear (Fig. 6). Different arm lengths have been prepared with a maximum
167 arm length of 62 cm, the arm length thereby being measured from the
168 pivot point of the rotation gear to the tip of the source holder. This arm
169 length allows the source to be placed in immediate contact with the cryo-
170 stat (Fig. 2, right), as the center axis of the organ pipe is 81 cm from the
171 TPC center and the cryostat has an outer radius of 32 cm. The 62 cm
172 arm was used for deployments in the past calibration campaigns (Sec. 4).
173 Inside the source holder the radioactive source is placed, pressed to the
174 tip and held in place via a spring during deployment, articulation and
175 dearticulation. The source holder is sealed such that no liquid scintillator
176 can enter during the deployment. This has also been verified during each
177 source extraction and no traces of liquid have been found on its inside.

178 *2.6. Hardware details and safety features*

179 CALIS offers various safety features to ensure that the device runs
180 smoothly, no components are lost inside the detector, avoid any contam-
181 ination of the detector by dirty or incompatible materials, maintain pres-
182 sure and avoid introduction of oxygen or water in contact with the LS
183 and TMB.

184 **Cable strength:** The cables holding the pig have been rated for loads over
185 1300 lbs, while the weight of the deployment device is at the level of
186 20-30 lbs so well below the breaking strength of the cable.

187 **Drive mechanism:** In the event of a power failure, the magnetic break
188 ensures there is no movement of the pig. The torque of the servo
189 motor is limited in case of an unexpected load.



Figure 6: Source holder that connects to an arm and to the articulation gear of the deployment device. The source, here a ^{133}Ba source, is pressed to the tip of the source holder via a spring.

190 The speed reducer (gears) is a double worm gear design. The pri-
 191 mary worm gear has a 50:1 reduction and the secondary worm has
 192 a 82:1 reduction. The input speed of the servo motor is 2400 RPMs
 193 and the output is 0.6 RPM and has the weight capacity of 148 lbs. In
 194 the event of a power failure the speed reducer has the ability to hold
 195 the load at any position without back drive. The speed of the motor
 196 has been limited to 0.4 cm/s which minimizes any lateral oscillation
 197 of the pig during lowering and raising the source. Additionally, this
 198 is the maximum speed at which the motor is not overheating.

199 **Manual retraction system:** In the unlikely case of a complete motor fail-
 200 ure while the source is deployed, it is possible to manually retract
 201 the pig back to its home position and close the gate valve. The mo-
 202 tor is disengaged, and a wrench is used to manually wind the cable
 203 back on the spools and retract the pig back above the gate valve.

204 **High limit switch:** A high limit switch is a hardware interlock, that pre-
 205 vents the deployment device to hit the cable spools and gears, should
 206 it pass beyond the home position in the CALIS housing (Fig. 5).

207 *Neither the manual retraction system had to be used so far nor has the high*
 208 *limit switch been activated during calibration campaigns.*

209 **Light and leak tightness of CALIS:** When the deployment device is next
 210 to the cryostat the gate valve is open and we take also data with the
 211 LSV. A prerequisite is that the housing is absolute light tight and

212 pressure leak tight. All view ports have light tight covers for when
 213 the organ pipe gate valve is open. Both light and leak tightness has
 214 been extensively validated throughout the manufacturing process
 215 until including commissioning (Sec. 3).

216 **Securing of the source:** All connection points for the source and arm
 217 have been secured with two push locking pins that cannot be dis-
 218 engaged without a person pressing the pin. In addition, the source
 219 holder and the two locking pins will all be tethered from outside the
 220 view port until they are locked in place eliminating the possibility
 221 of accidental falling into the inside of the CALIS housing.

222 *2.7. Degrees of freedom of the system*

223 CALIS has the capability to deploy sources at various positions inside
 224 the LSV. Besides the movement along z up to the maximum cable length,
 225 there is the possibility to articulate at an angle of θ between 90° and 180° ,
 226 where θ is the zenith-angle (Fig. 7). Degrees between 0° and 90° are
 227 excluded because the end of the articulation chain is reached at an angle
 228 of 90° (see Fig. 3).

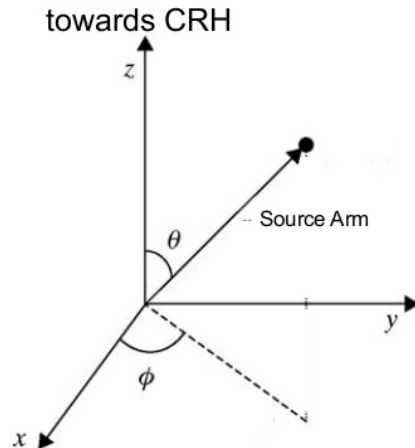
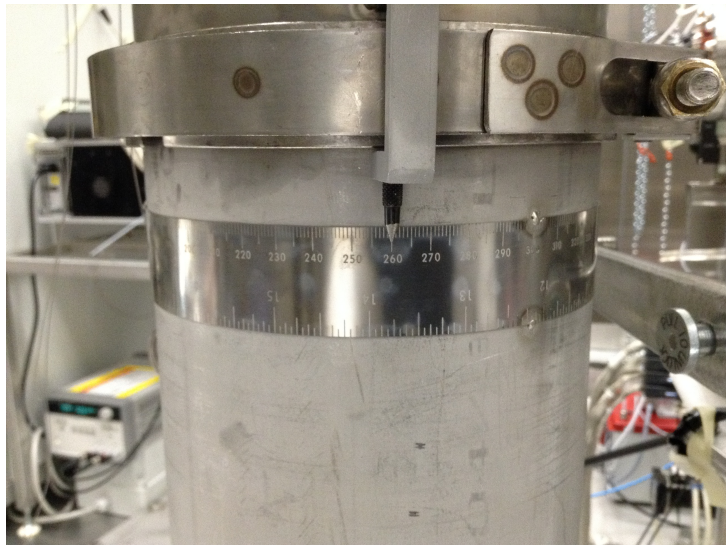


Figure 7: Spherical coordinate system used for establishing the direction of the rotation of CALIS-III and the articulation of the source arm. θ is kept at 90° when arm is articulated, and at 180° when dearticulated. x-axis is the direction toward the center of the detector.

229 2.7.1. *Rotation in the XY plane*

230 Below the view port is a sealed connection that has an o-ring seal
231 and uses a ring clamp to compress the seal. The clamp can be slightly
232 loosened to allow the upper assembly (above and including the view port)
233 to be rotated with respect to the lower assembly and the detector. This
234 rotation in the XY plane can even be performed while the deployment
235 device is deployed next to the cryostat, since the seal is helium leak and
236 light tight even when loosened.

237 In principle a rotation in 360° can be done, except when the arm would
238 interfere with the cryostat. This has been used in one of the calibration
239 campaigns to deploy a neutron source directly next to the cryostat and
240 rotated away by 90° in order to study optical shadowing effects from the
241 cryostat (Sec. 4).



My impression is that a drawing to scale with the cryostat, the TPC the organ pipe and the source arm would be good here

Figure 8: Underneath the view port is the ring clamp with the angle measuring strip underneath. In order to perform azimuthal rotation, the ring clamp is slightly loosened, and the entire upper assembly is rotated with respect to the lower assembly, along with the deployment device. The angle of rotation is read from the strip that goes around the pipe. The strip is in mm, which has then been calibrated in degrees.

242 2.7.2. “No fly” zone

243 Right above the cryostat where there are many supply tubes for the
244 TPC a “no fly” zone has been defined. In this region no part of the
245 deployment device may enter, in particular not the source arm.

246 2.7.3. *Default configuration*

247 By default the deployment device has been deployed with the longest
248 arm (62 cm), at the center of the active volume of the TPC, with the arm
249 rotated in the XY plane until contact with the cryostat has been made.

250 Other degrees of freedom could involve shorter arm lengths, while
251 longer arm lengths have been discussed but would require hardware
252 modifications to the deployment device. Out of a total of four organ
253 pipes a second one would be available for source calibration. (Two organ
254 pipes are not available due to interference with existing infrastructure:
255 the cryogenic tower and electronic rack.) A change in organ pipe would
256 require a bigger effort involving a partial disassembly of CALIS and re-
257 installation on the other organ pipe's gate valve.

258 **3. Testing, Cleaning and Commissioning**

259 CALIS has been assembled at FNAL from components produced at
260 FNAL and University of Hawaii. After an initial set of basic functional-
261 ity tests at FNAL, CALIS was shipped pre-assembled to LNGS, where it
262 would undergo a comprehensive testing and calibration program. Still
263 outside the clean room CRH, CALIS was installed on a high bay and
264 tested at its full length. Besides testing all details of CALIS (see Sec. 2.6)
265 ranging from testing the functionality of motor controls, high limit and
266 articulation switch to recovery scenarios after e.g. power failures during
267 deployment.

268 An important aspect was the calibration of the sources Z-position as a
269 function of cable length before and after articulation of the source, which
270 is a nonlinear function of motor step counts, as mentioned in Sec. 2.2. Fur-
271 thermore the accuracy and precision of XY- and Z-position of the source
272 was estimated.

273 The results of this testing campaign were reviewed by an internal re-
274 view board and approval for installation inside CRH was granted. CALIS
275 was cleaned according to official cleaning procedures and installed on the
276 gate valve of CRH in September 2014. After installation on the gate valve
277 a focus of testing was the light and helium leak tightness of the system,
278 and the testing of the nitrogen and vacuum systems, as these could only
279 be tested in full after installation. A more detailed description of tests
280 performed at FNAL and LNGS can be found in [5, 6].

Tests will be
described in
more detail in
Erin and Bri-
anne's thesis
→ cite them
here.

281 XY and Z position

282 Tests in air and in the LSV's scintillator revealed that the source po-
283 sition accuracy and precision is dominated by uncertainties during artic-
284 ulation. The positioning in z before articulation is highly accurate and
285 precise: The deployment speed is very low, barely visible to the naked
286 eye (4 mm/s), which minimizes the lateral motion during deployment
287 and contact with housing or organ pipe is avoided during deployment.
288 Yet during articulation a swing in XY is arising from tiny laterally imbal-
289 anced forces originating in the pull on the articulating cable.

290 To ensure deployment precision we worked out a procedure to make
291 reliably gentle contact with the cryostat, thereby eliminating the preci-
292 sion uncertainty in XY: After positioning the deployment device in z, the
293 source arm is articulated to horizontal while it is pointing away from the
294 cryostat. Only then the source is brought into contact with the cryostat
295 through a rotation in XY while monitoring the PMT scaler rates, which
296 increase while the source is approaching, yet plateaus as soon as contact
297 with the cryostat is made, even if the rotation in XY continues. This pro-
298 vides a reliable XY and Z-position for the calibration source and has been
299 used throughout calibration campaigns.

300 **4. Calibration Campaigns**

301 *4.1. Radioactive Sources*

302 For the calibration of the LSV detector response and the TPC's re-
303 sponse to electron recoils (ER) we selected ^{57}Co , ^{133}Ba and ^{137}Cs . In a
304 later calibration campaign also ^{22}Na has been deployed. They allow a
305 cross-calibration with ^{83m}Kr , that has been injected in the Ar recirculation
306 system during dedicated campaigns and the internal ^{39}Ar , as they cover
307 the energy range of ^{39}Ar (see also Table 1 and Fig. 9).

308 After a preselection of gamma source energies, detailed studies with
309 the DarkSide Monte Carlo simulation package G4DS [?] were per-
310 formed to select appropriate source activities and check the feasibility
311 and physics reach of various deployment positions. Considering also
312 constraints from the LSV and TPC DAQs, sources with suitable activities
313 were identified for deployment (Table 1).

314 Energy variables are calibrated in photo-electrons (PE) using dedi-
315 cated Laser calibration runs, in which the single PE charge spectra for
316 each PMT are fitted and a PE-charge gain is determined. These Laser

possible
upgrade for
fig.16:
measured
spectra
overlaid
at a fixed
HV: 83mKr,
 $\text{Co}57$, $\text{Ba}133$,
 $\text{Cs}137$ (either
null field or
200 V/cm) -
ask Brianne?
Also for her
thesis?

317 runs are also an integral part of a calibration campaign requiring a Laser
 318 run every few hours and at least on each change in DAQ or CALIS con-
 319 figuration, such as drift field changes or source position changes.

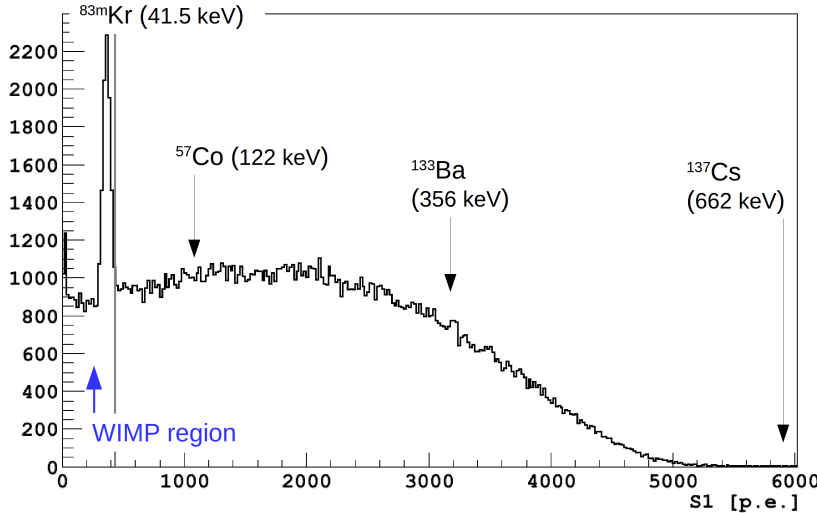


Figure 9: Scintillation spectrum (S1) at null field showing a ^{83m}Kr peak on the ^{39}Ar β spectrum. The energies of the three gamma sources are indicated and cover the full range of the ^{39}Ar spectrum.

320 4.2. Timeline of the Calibration Campaigns and Stability

321 Between October 2014 and April 2016 the following calibration cam-
 322 paigns have been performed:

- 323 • The first extensive campaign involving all gamma sources and both
 324 the high and low activity AmBe neutron source took place in Octo-
 325 ber and November 2014 at LNGS. The TPC was filled with Atmo-
 326 spheric Argon with an inherent trigger rate of approx. 50 Hz from
 327 ^{39}Ar . The liquid scintillator of the LSV contained a PC only scintilla-
 328 tor with $< 0.1\%$ TMB and 1.4 g/l PPO as wavelength shifter.
- 329 • In January and February 2015 a second campaign focusing on the
 330 LSV calibration using the low activity AmBe source was performed.
 331 Prior to that the LSV has been reconstituted with 5 % TMB. Two
 332 deployments were performed at two different PPO concentrations

get the num-
bers for Na22
in the table

has atmo-
spheric argon
been intro-
duced and
underground
argon?

what does
5 % TMB
mean?
weight %,
volume %?

Table 1: Gamma sources deployed in DS-50, ^{39}Ar and $83m\text{Kr}$ [?]. Interaction length is in LAr. Activity of ^{39}Ar has been approx. 50 Hz during AAr filling and negligible in the UAr phase. The Kr source activity varied from campaign to campaign, but was in the range of a few Bq to some tens of Bq.

source	type	energy	half life	interact. length	activity
^{57}Co	γ	122 keV	0.744 y	4.4 cm	35 kBq
^{133}Ba	γ	356 keV	10.54 y	7.5 cm	2 kBq
^{137}Cs	γ	662 keV	30.2 y	9.5 cm	0.65 kBq
^{22}Na	γ	$2 \cdot 511 \text{ keV} + 1274 \text{ keV}$	xxx y	xxx cm	11 kBq
^{39}Ar	β	565 keV endpoint	xxx y	sub-mm	50 Hz
^{83m}Kr	2β	$32.1 \text{ keV} + 9.1 \text{ keV}$	xxx y	sub-mm	

(0.7 g/l and 1.4 g/l), allowing to study the impact of the PPO concentration on alpha and gamma quenching. (1.4 g/l is our nominal PPO concentration, see also Fig. 14, right)

- In August 2015 a ^{22}Na source has been deployed next to the cryostat for TPC calibration. This was the first gamma source calibration campaign after the UAr deployment within DarkSide-50.
- In December 2015 an $^{241}\text{Am}^{13}\text{C}$ neutron source has been deployed, allowing an in-depth study of the detection efficiency of the prompt neutron recoil signal in the absence of the correlated 4.4 MeV gamma, obfuscating the neutron recoil signal in case of an AmBe source.

As shown in Fig. 10 the calibration campaigns have not affected negatively the light yield or introduced radioactivity into the LSV.

4.3. TPC Calibration

A few calibration results are shown to illustrate the quality of the acquired calibration data and their description in G4DS [?].

4.3.1. ^{57}Co S1 energy

Fig. 11 shows a data-MC comparison of the scintillation signal S1 spectrum of a ^{57}Co calibration source deployed next to the cryostat and close to the TPC active volume center. Overlayed is the S1 distribution from an equivalent selection of G4DS MC simulation.

instead of
the timeline
by Yann
(DocDB

1232) I
would like
to show the
Co60 and a
rate stability
plot - in
progress.

The plot is
from Paolo's
G4DS talk
DS2016,
UCLA.
Ideally one
could get an
official copy
from the MC
paper.

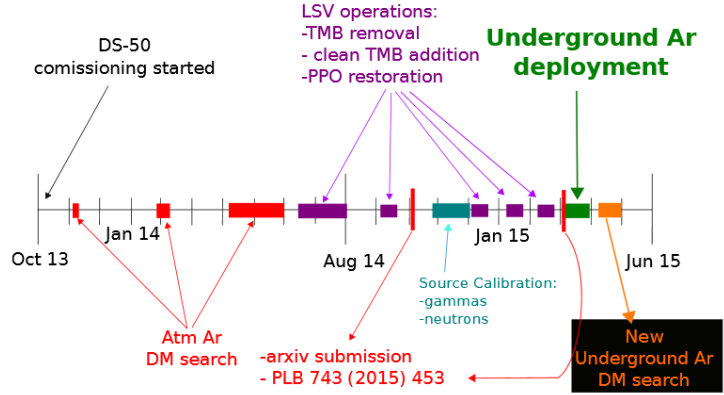


Figure 10: In black the stability of the LSV LY is monitored using internal ^{60}Co emitted from the cryostat steel, in blue the stability of the rate of radioactivity in the LSV is shown. Before and after calibration campaigns both the LY and the rate remain unaffected.

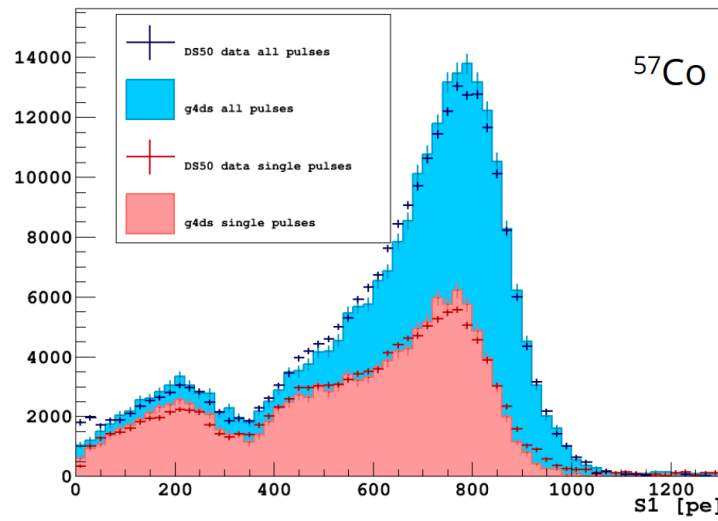


Figure 11: Data-MC comparison for the ^{57}Co source deployed next to the cryostat. In the magenta distribution a single-site interaction requirement has been imposed as for dark matter events and for the blue distribution this constraint has been removed [?].

353 4.3.2. *F90 distribution from $^{241}\text{Am}^9\text{Be}$ neutron data*

354 Fig. 12 shows good agreement between F90 medians and S1 spectra
 355 measured from $^{241}\text{Am}^9\text{Be}$ neutron data and those derived from SCENE
 356 measurements, which have been used to determine the nuclear recoil en-
 357 ergy scale and NR acceptance regions for the WIMP dark matter search
 [? ?].

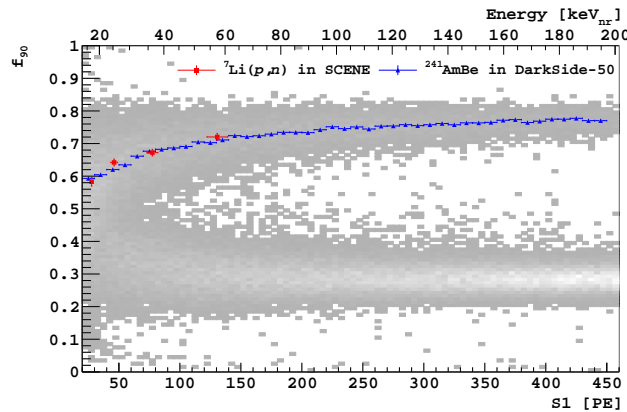


Figure 12: Plot of F90 vs. scintillation signal S1 from a high rate AmBe neutron source calibration of DarkSide-50 in grey, the upper NR band from the AmBe calibration and lower ER band from β - γ backgrounds are visible. Overlayed are f_{90} NR median vs. S1 from a high-rate *in situ* AmBe calibration (blue) and scaled from SCENE measurements (red points) [?]. There is very good agreement between the two. The high source intensity and correlated neutrons and γ -ray emission by the AmBe source contribute events outside the nuclear recoil and electron recoil bands. (reproduced from [?])

358

359 4.3.3. *Source position*

360 Tests at LNGS established the deployment system's positioning accu-
 361 racy to be about ± 1 cm after a 7 meter journey into the DarkSide-50 LSV.
 362 During the first calibration campaign several runs have been taken with
 363 the source at its central position (731000 motor step counts). Fitting the
 364 t_{drift} distribution at that position for a sequence of runs a systematic shift
 365 vs. time has been observed (Fig. 13, right). The source position has been
 366 on average 157.4 mm below the grid with an RMS of 10.1 mm. Follow-
 367 ing that observed systematic shift with time the deployment procedures
 368 have been revised to avoid such a time dependency in the future and to
 369 improve the deployment precision. It is worth mentioning though that
 370 this does not induce significant uncertainties for calibration data analy-

ses, as the t_{drift} distribution can be measured in-situ on a per-run basis and hence does not affect our dark matter analysis.

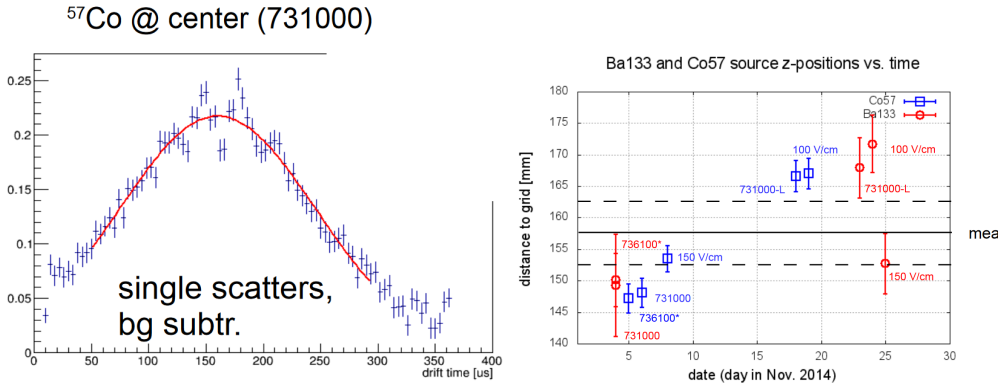


Figure 13: *left*: A t_{drift} distribution encoding the z-position of the ^{57}Co deployed next to the TPC center. *right*: Shift of source position relative to the TPC grid as a function of time when deployed to the same place.

For the XY position the distribution of the azimuthal angle in the XY plane has been studied and a mean of 139 degrees has been observed with an RMS of 1.2 deg. (One degree corresponds to 6 mm at the outer cryostat, where the source is positioned.) However an independent XY reconstruction algorithm gave 142.5 degrees with an RMS of 0.8 deg, so that systematic uncertainties from the reconstruction dominate over the XY precision [?].

4.4. Liquid Scintillator Veto

In Fig. 14 (left) a data-MC comparison of the LSV charge spectra from the ^{137}Cs source deployed in the LSV next to the cryostat is shown [?]. In January and February 2015 the reconstitution of the LSV scintillator was completed and a second AmBe neutron source calibration of the LSV calibration was undertaken to further study the various neutron detection channels in the LSV. With a borated scintillator, a critical aspect of the neutron detection efficiency is the capability to observe the 6.4 % capture branch leading to a 1775 keV $\alpha + ^7\text{Li}(\text{g.s.})$ without the accompanying 478 keV γ -ray. As shown in Fig. 14 (right) the de-excitation channel is clearly observed at around 30 PE.

This is from DocDB 1288. Ideally one could cite a XY paper here, which is not published yet.

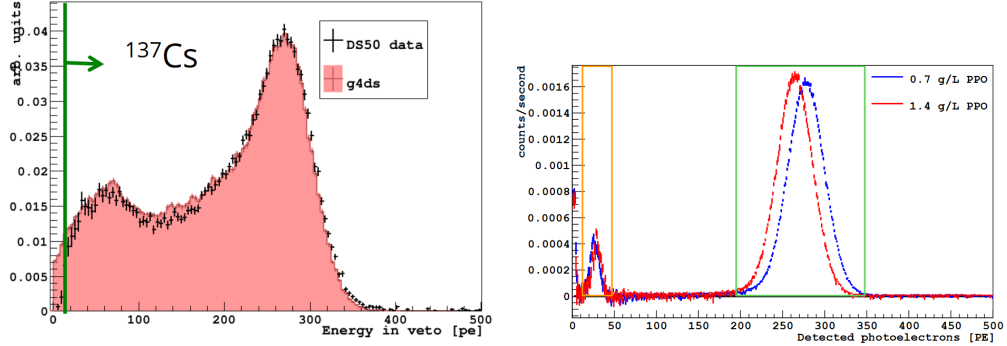


Figure 14: *left:* Data-MC comparison of the LSV charge spectra from the ^{137}Cs source deployed in the LSV next to the cryostat [?]. *right:* Clear detection of the neutron capture signal on ^{10}B in the LSV leading to a 1775 keV $\alpha + ^7\text{Li}(\text{g.s.})$ at ≈ 30 PE (orange box). The peak on the right at ≈ 270 PE (green box) is from the 93.6 % of captures that lead to the ^7Li excited state reaction, with the accompanying 478 keV-ray. The entries below 10 PE are due to PMT after-pulses. Data has been taken before and after varying the concentration of the wavelength shifter PPO in the scintillator with the source rotated 70 cm away from the cryostat. In both cases the deexcitation to ground state is clearly observed.[?]

391 5. Conclusions

392 summarize that the LSV and TPC detector have not been negatively
393 affected.

394 Refer to the next generation DS-detector.

- 395 [1] P. Agnes, et al., *First results from the DarkSide-50 dark matter experiment*
396 *at Laboratori Nazionali del Gran Sasso*, Phys. Lett. B, **743**, 456 (2015).
- 397 [2] P. Agnes and Others, *The veto system of the DarkSide-50 experiment*,
398 JINST, **11**, P03016 (2016).
- 399 [3] T. I. Banks and Others, *A compact ultra-clean system for deploying ra-*
400 *dioactive sources inside the KamLAND detector*, Nucl. Instrum. Meth.,
401 A**769**, 88 (2015).
- 402 [4] H. X. Huang and Others, *Manual Calibration System for Daya Bay Reac-*
403 *tor Neutrino Experiment*, JINST, **8**, P09013 (2013).
- 404 [5] B. Hackett, *[thesis title]*.
- 405 [6] E. Edkins, *[thesis title]*.